Published in final edited form as:
Nat Med. 2013 February ; 19(2): 209–216. doi:10.1038/nm.3043.

Recoding RNA editing of *antizyme inhibitor 1* predisposes to hepatocellular carcinoma

Leilei Chen[1,2,3,*], **Yan Li**[1,3,*], **Chi Ho Lin**[4], **Tim Hon Man Chan**[1,2,3], **Raymond Kwok Kei Chow**[1], **Yangyang Song**[1,3], **Ming Liu**[1,3], **Yun-Fei Yuan**[5], **Li Fu**[1], **Kar Lok Kong**[1], **Lihua Qi**[2], **Yan Li**[5], **Na Zhang**[4], **Amy Hin Yan Tong**[4], **Dora Lai-Wan Kwong**[1], **Kwan Man**[6], **Chung Mau Lo**[6], **Si Lok**[4], **Daniel G. Tenen**[2], and **Xin-Yuan Guan**[1,3,5]

[1]Department of Clinical Oncology, Li Ka Shing Faculty of Medicine, The University of Hong Kong, Hong Kong, China

[2]Cancer Science Institute of Singapore, National University of Singapore, Singapore

[3]State Key Laboratory of Liver Research, Li Ka Shing Faculty of Medicine, The University of Hong Kong, Hong Kong, China

[4]Genome Research Centre, Li Ka Shing Faculty of Medicine, The University of Hong Kong, Hong Kong, China

[5]State Key Laboratory of Oncology in Southern China, Sun Yat-sen University Cancer Center, Guangzhou, China

[6]Department of Surgery, Li Ka Shing Faculty of Medicine, The University of Hong Kong, Hong Kong, China

Abstract

Better understanding of human hepatocellular carcinoma (HCC) pathogenesis at the molecular level will facilitate the discovery of tumor initiating events. Herein, transcriptome sequencing revealed that adenosine (A)-to-inosine (I) RNA editing of *antizyme inhibitor 1* (*AZIN1*) displays a high modification rate in HCC specimens. A-to-I editing of *AZIN1* transcripts is specifically regulated by a*denosine deaminase acting on RNA-1 (ADAR1)*. The serine (S) → glycine (G) substitution at residue 367, located in β-strand 15 (β15), predicted a conformational change, induced a cytoplasmic-to-nuclear translocation, and conferred "gain-of-function" phenotypes manifested by augmented tumor initiating potential and more aggressive behavior. Compared with wild-type AZIN1 protein, the edited form possesses stronger affinity to antizyme, and the resultant higher protein stability promotes cell proliferation via the neutralization of antizyme-mediated degradation of ornithine decarboxylase (ODC) and cyclin D1 (CCND1). Collectively, A-to-I RNA

Correspondence should be addressed to: Professor Xin-Yuan Guan, PhD, Department of Clinical Oncology, Li Ka Shing Faculty of Medicine, The University of Hong Kong, Room 56, 10/F, Laboratory Block, 21 Sassoon Road, Pok Fu Lam, Hong Kong. Tel: (852) 2819-9785; Fax: (852) 2816-9126; xyguan@hkucc.hku.hk. Daniel G. Tenen, Cancer Science Institute of Singapore, #12-01, MD6, Centre for Translational Medicine, 14 Medical Drive, Singapore 117599; csidgt@nus.edu.sg.
*These authors contributed equally to this work.

AUTHOR CONTRIBUTIONS

L.C., Y.L., and X.Y.G. initiated and designed the study. L.C. wrote the manuscript with input from D.G.T. and X.Y.G. L.C., Y.L., and C.L. designed the experiments and interpreted the results. L.C. and Y.L. performed all experiments with assistance from T.C., Y.S., M.L., L.Q., and R.C. Illumina mRNA library preparation was performed by N.Z. and A.T. C.L. and S.L. performed all bioinformatics analysis of transcriptome sequencing. HCC clinical sample and the relevant clinical information were provided by Y.F.Y. and extracted by L.C. and Y.L. Healthy human liver tissues were provided by K.M. and C.M.L. Human PBMCs were collected by L.F. NPC samples were provided and extracted by D.K., K. K., and L.C. D.G.T and X.Y.G. supervised the project.

COMPETING FINANCIAL INTERESTS

The authors declare no competing financial interests.

editing of *AZIN1* may be a potential driver in the pathogenesis of human cancers, particularly HCC.

Keywords

A-to-I; RNA editing; AZIN1; ADAR1; antizyme; ODC; CCND1; HCC

INTRODUCTION

Hepatocellular carcinoma (HCC) represents the third most common cause of cancer-related deaths worldwide with a dismal clinical outcome [1]. Like other solid tumors, HCC development is believed to be a multi-step process with the accumulation of genetic and epigenetic alterations[2,3]. The recent advent of genomic tools, including RNA sequencing (RNA-Seq), has provided powerful tools to study changes in transcriptomes and genomes to understand cancers at the molecular level[4–6].

In this study, we performed an integrative RNA-Seq analysis on three pairs of HCC and their matched non-tumor (NT) tissue counterparts and identified an adenosine (A)-to-inosine (I) RNA editing event involved in HCC progression. In humans, the most frequent type of RNA editing is conversion of adenosine (A) to inosine (I) with the splicing and translational machineries subsequently recognizing the inosine (I) as a guanosine (G). We found A-to-I RNA editing over-occurring at codon 367 of *AZIN1* (antizyme inhibitor 1), resulting in a serine (Ser) to glycine (Gly) amino acid substitution in approximately 50% of primary HCC samples. A-to-I (G) editing is mediated by the double-stranded RNA (dsRNA)-specific ADAR (adenosine deaminase acting on RNA) family[7]. In this study, we demonstrate that ADAR1-mediated *AZIN1* RNA editing is linked to tumor initiation and development.

RESULTS

A close link between *AZIN1* overediting and HCC pathogenesis

In order to detect abnormal single nucleotide variations (SNVs) during neoplastic transformation, we applied high-throughput RNA-Seq to investigate three pairs of HCC tumor and their adjacent non-tumor (NT) tissues, identifying 94, 89, and 101 coding somatic single nucleotide variants (cSNVs) in the three tumor samples (Supplementary Data, Supplementary Tables 1–4, and Supplementary Fig. 1a–c). Validation analysis was performed for 10 of the intersecting cSNVs (all are non-synonymous substitutions), and the majority were confirmed (Supplementary Data and Supplementary Fig. 1d, e). By genotyping validation of the DNA samples, *antizyme inhibitor 1* (AZIN1) demonstrated a high frequency of non-synonymous A-to-I transcript editing, leading to a serine (Ser) to glycine (Gly) amino acid substitution (Supplementary Data and Supplementary Fig. 1f–h). A-to-I (G) editing of *azin1* was detected in mouse (*Mus musculus*) liver tissue, and a 100 bp region in intron 11 immediately downstream of exon 11 is conserved, especially the first 16 bp (100% identity). We hypothesized that the *AZIN1* transcript would undergo A-to-I editing by a mechanism similar to that occurring in *GluR-B* transcripts[8,9]; this RNA secondary structure may juxtapose the *AZIN1* editing site and the potential exon complementary sequence (ECS) for A-to-I conversion (see Supplementary Data and Supplementary Fig. 2).

We investigated *AZIN1* editing levels in 135 matched primary HCC and non-tumor (NT) liver tissues from Guangzhou, China (GZ cohort) and 46 matched primary HCC and NT liver samples from Shanghai, China (SH cohort). Approximately 46.7% (63/135 of GZ patients) and 50.0% (23/46 of SH patients) of the primary HCC specimens demonstrated

AZIN1 overediting, defined by an increase of not less than 10% editing level in tumors compared to adjacent NT specimens (Fig. 1a).

AZIN1 editing levels were found to be significantly higher in healthy liver tissues than in peripheral blood mononuclear cells (PBMCs) ($P = 0.0007$) and in other normal tissues (Fig. 1b and Supplementary Fig. 3). Intriguingly, the degree of *AZIN1* editing gradually increased during HCC pathogenesis from normal to adjacent NT to clinically verified HCC (Fig. 1b). HCC patients with liver cirrhosis demonstrated higher *AZIN1* editing frequency than those without liver cirrhosis (37.13 *vs.* 28.93%; $P = 0.0052$), and also higher in HCC patients with tumor recurrence than those without (36.99 *vs.* 31.12%; $P = 0.012$, Fig. 1b). Clinicopathological analyses demonstrated that *AZIN1* overediting in tumors was significantly correlated with the presence of liver cirrhosis ($P = 0.003$), tumor recurrence ($P = 0.001$), and worse prognoses ($P_{Disease\text{-}free} = 0.008$) (Fig. 1c–e and Supplementary Tables 5 and 6). In summary, *AZIN1* editing frequency increases during progression from cirrhosis and primary liver cancer to advanced HCC with recurrence and metastasis.

ADAR1 is responsible for *AZIN1* RNA editing in human cancers

Based on our RNA-Seq, the two *ADAR1* transcript variants (NM_001025107 and NM_015840), encoding 110 kDa (p110) and 150 kDa (p150) isoforms, respectively, demonstrated relatively high abundances in liver tissue. Other family members were expressed either at extremely low (*ADAR2*) or undetectable (*ADAR3*) levels (Supplementary Fig. 4a–c).

We further examined expression levels of ADAR1-3 in clinical specimens of 94 HCC patients from the GZ cohort. *ADAR3* could not be detected in any of the samples, and there was an approximate five-cycle difference in the average delta cycle threshold (Ct) between *ADAR1* and *ADAR2*, indicating that the *ADAR1* expression level was 32-fold higher than that of *ADAR2* in the human liver samples (Supplementary Fig. 4d). Both ADAR1 p110 and p150 isoforms were upregulated in 83% (25/30) of HCC cases, predominantly the p110 isoform (Fig. 2a). *AZIN1* editing frequency was positively correlated with *ADAR1* and not *ADAR2* (Fig. 2b, c). Similar to HCC, the editing level and expression of *ADAR1* in esophageal squamous cell carcinoma (ESCC) were significantly higher than in adjacent NT tissues ($P < 0.0001$, Fig. 2d), which may be explained by the higher *ADAR1* expression level (as shown by a lower Ct value) in HCC and ESCC tumor samples compared with the matched NT tissues (Fig. 2e). No obvious differences in the *AZIN1* editing level and *ADAR1* expression were detected between the tumor and NT tissues of nasopharyngeal carcinoma (NPC) (Fig. 2d, e). These data suggested that *ADAR1* plays the major role in A-to-I (G) *AZIN1* editing during cancer development.

Because of its regulation by interferon (IFN) and cytoplasmic localization, the ADAR1 p150 is presumably responsible for A-to-I editing of viral RNAs produced by viruses[7,10] but not nuclear pre-mRNAs[11]. Overexpression of *ADAR1* p110 but not *ADAR2*, led to a five-fold increase in *AZIN1* editing (Fig. 2f–h). Silencing *ADAR1* in the HCC cell line H2M dramatically decreased *AZIN1* editing and was rescued by overexpressing an *ADAR1* p110 mutant (Fig. 2i, j). In summary, studies of expression of ADAR family members and functional studies support the notion that *ADAR1* p110 serves to induce *AZIN1* overediting.

AZIN1 A-to-I (G) editing induces a tumorigenic phenotype

To ascertain whether there is a causative relationship between RNA editing and "gain-of-function" phenotypes in cancer development, we introduced V5-tagged wild-type (wt/AZI) or edited *AZIN1* (edt/AZI) expression constructs into two HCC cell lines (PLC8024 and QGY7703). Wt/AZI and edt/AZI lentivirus-transduced cells demonstrated accelerated

growth rates and higher frequencies of focus and colony formation in soft agar than controls (8024-LacZ and 7703-LacZ) (Fig. 3a–c). In spite of similar levels of expression (Supplementary Fig. 5a, b), cells expressing edited AZIN1 (i.e., 8024-edt/AZI and 7703-edt/AZI) with 84–90% of their *AZIN1* transcripts edited (Supplementary Fig. 5c), demonstrated greater tumorigenic properties than cells expressing wild-type (8024-wt/AZI and 7703-wt/AZI) (Fig. 3a–c). Consistent with the clinical correlation between *AZIN1* overediting and tumor recurrence, edt/AZI lentivirus-transduced cells possessed increased invasive capability (Fig. 3d).

To analyze if the "gain-of-function" phenotypes are regulated in an edited AZIN1-dependent manner, we compared the tumorigenic properties of wt/AZI-transfectant (8024-Wt1) with three edt/AZI–transfectants (8024-Edt1, 2 or 3) with different *AZIN1* editing frequencies (24.8%, 42.9% and 85.3%). 8024-Edt3 cells, harboring 85.3% edited *AZIN1* transcripts, demonstrated the most aggressive phenotype (Fig. 3e–h). As little as an 18% increase in *AZIN1* editing level (compare 8024-Edt1 and 8024-Edt2 cells) was sufficient to promote tumorigenic potential (Fig. 3e–h). These data demonstrate that tumorigenic properties correlate with *AZIN1* editing levels.

Xenograft studies demonstrated that the tumor incidence induced by 8024-edt/AZI cells was dramatically higher than those induced by 8024-wt/AZI and 8024-LacZ (Fig. 4a, b). Moreover, 70% of mice injected with 8024-edt/AZI cells formed tumors within one week; however, none of the mice injected with 8024-LacZ and only 10% with 8024-wt/AZI had visible tumors (Fig. 4a, b). Tumors induced by 8024-edt/AZI cells grew significantly faster than those induced by 8024-LacZ or 8024-wt/AZI cells (Fig. 4c). Furthermore, 4 weeks following intrahepatic inoculation, mice injected with 8024-edt/AZI cells formed more liver nodules (Fig. 4d–f). All these data demonstrate that this recoding editing plays a significant role in tumor initiation.

AZIN1 editing causes a cytoplasmic-to-nuclear translocation

Editing of *AZIN1* results in an amino acid change (Ser Gly) of residue 367. GFP-tagged wild-type AZIN1 protein (GFP-wt/AZI) was predominantly expressed in the cytoplasm, whereas the majority of the edited protein (GFP-edt/AZI) was expressed in the nucleus (Fig. 5a). The centrosomal localization of wild-type AZIN1 protein was observed as reported previously[12] (indicated by arrows, Fig. 5a). Despite equal amounts of GFP-wt/AZI and GFP-edt/AZI in whole cell lysates, cytoplasmic GFP-wt/AZI protein was four-fold higher than cytoplasmic GFP-edt/AZI protein, while edited AZIN1 protein was four-fold more abundant in the nuclei, indicating that the *AZIN1* editing may result in a cytoplasmic-to-nuclear translocation (Fig. 5b). By immunohistochemistry (IHC), cytoplasmic-to-nuclear translocation of AZIN1 was observed in 5/14 (35.7%) cases with *AZIN1* overediting (Fig. 5c).

We hypothesized that this translocation might be due to a conformational change as a result of Ser Gly substitution at the residue 367. To this end, we used computational methods to identify predicted conformationally switching elements in the AZIN1 protein. Intriguingly, the program ASP (Ambivalent Structure Predictor)[13] identified two individual switching elements (Switch I: residues 362–367; and Switch II: residues 385–394) from the 448-aa protein sequence (Fig. 5d), highly suggesting that amino acid change within these two elements could be involved in the conformational change in AZIN1. Intriguingly, the residue Ser367 locates right at the "Switch I" region, suggesting that a Ser Gly substitution at residue 367 might have the potential to induce a conformational change in AZIN1.

Edited AZIN1 neutralizes antizyme-mediated degradation of oncoproteins

Antizyme inhibits cell growth by binding to and inducing degradation of proteins such as ODC. AZIN1 is an ornithine decarboxylase (ODC) homolog and shares its capacity to bind to antizyme, but AZIN1 binds to antizyme with a higher affinity than ODC[14]. Compared with GFP-tagged wild-type *AZIN1* (GFP-wt/AZI)-transfected cells, more antizyme-1 protein could be pulled down from the lysates of cells transfected with GFP-tagged edited *AZIN1* (GFP-edt/AZI) (Fig. 6a). Also, we observed that more antizyme-1 protein could be immunoprecipitated in 8024-edt/AZI cells compared with 8024-wt/AZI cells using a V5-specific antibody (Supplementary Fig. 6a). Furthermore, an equal amount of recombinant maltose-binding protein (MBP)-fused antizyme-1 (MBP-OAZ1) protein could pull down more GFP-edt/AZI protein than GFP-wt/AZI (Fig. 6b). All of these data indicated that the edited AZIN1 possessed higher binding affinity to antizyme-1 than wild-type AZIN1.

As a consequence of its increased binding affinity to antizyme, edited AZIN1 protein was more stable than wild-type form (Fig. 6c, d and Supplementary Fig. 6b–d), consistent with previous findings that the AZIN1/antizyme-1 interaction prevents AZIN1 from undergoing ubiquitin-mediated degradation[15].

Binding of AZIN1 inhibits antizyme-mediated binding and degradation of the ODC and cyclin D1 (CCND1) oncoproteins[16–18]. ODC and CCND1 degradation was attenuated in cells expressing GFP- or V5-tagged edited AZIN1 compared with cells expressing wild-type AZIN1 (Fig. 6c, d and Supplementary Fig. 6b–d). Therefore, *AZIN1* editing confers greater stability through higher affinity to antizyme-1, inducing malignant transformation by neutralizing antizyme-mediated degradation of downstream oncoproteins.

A functional edt/AZI-ODC/CCND1-cell proliferation axis in tumor progression

The promotion of cell proliferation is a major mechanism associated with the transformation of a normal cell to a cancer cell[19], and ODC and CCND1 are two key factors in regulation of the G1/S transition. Elevated ODC and CCND1 levels at the G1/S boundary lead to the augmentation of protein synthesis that is necessary for entry into the cell cycle[20,21].

We isolated tumorigenic cells from xenografts induced by 8024-wt/AZI and 8024-edt/AZI cells (xeno-wt/AZI & xeno-edt/AZI) and measured G1/S transition and cell proliferation using bromodeoxyuridine (BrdU) incorporation. Xeno-edt/AZI cells, displaying 13-fold higher *AZIN1* editing frequency, entered S phase faster than xeno-wt/AZI cells (Supplementary Fig. 7a, b). The percentage of xeno-edt/AZI cells in S phase was consistently higher than that of xeno-wt/AZI cells at 6 and 9 hours post-release (Fig. 6e). At the G1/S boundary, phosphorylation of the retinoblastoma protein (Rb) activates the E2F transcription factor and downstream targets such as cyclin A (CCNA), Cdc2, and c-Myc[22]. Compared with xeno-wt/AZI cells, xeno-edt/AZI cells had elevated ODC and CCND1, leading to increased Rb phosphorylation and subsequent upregulation of CCNA (Fig. 6f, g). Furthermore, as detected by IHC staining, xenograft tumors derived from 8024-edt/AZI cells demonstrated cytoplasmic-to-nuclear translocation of AZIN1 and higher expression of ODC, CCND1, and the proliferation marker KI67 than tumors derived from 8024-wt/AZI cells (Supplementary Fig. 7c). These data suggest that there is a tight connection between the edt/AZI-ODC/CCND1-cell proliferation axis and tumor initiation and progression.

DISCUSSION

RNA editing is defined as post-transcriptional alteration of RNA sequences and serves as an additional epigenetic control mechanism[23–25]. Until recently, only a small number of proteins with amino acid substitutions caused by editing were known, and it seems that many of the newly identified recoding events display low-level modification rates and low

validity[26,27]. In this study, RNA editing of *AZIN1* gene demonstrated a relatively higher modification ratio, and the accumulation of a Ser367Gly substitution was detected in tumor specimens, particularly HCCs.

In contrast with the notion that hypoediting is associated with several cancer phenotypes[28–30], we observed that *AZIN1* editing increased during the multistep progression of HCC from healthy and non-cancerous liver to HCC. Moreover, the *AZIN1* overediting in tumors was predictive of poor prognosis and associated with liver cirrhosis and tumor recurrence. Three ADARs (ADAR1, ADAR2 and ADAR3) have been identified to catalyze A-to-I RNA editing[31]. However, no substrate for *ADAR3* has been identified so far. We demonstrated that RNA editing of *AZIN1* was specifically regulated by *ADAR1* but not *ADAR2* and *ADAR3*. Moreover, *AZIN1* RNA editing was found to be conserved, implying that *cis*-acting sequences necessary for RNA editing should also be conserved. Computer programs that predict RNA secondary structures aligned the highly conserved exonic sequence with the intronic sequence immediately downstream of the edited exon within a highly base-paired dsRNA secondary structure. A series of assays both in cell culture and xenografts provided direct evidence that edited AZIN1 protein confers "gain-of-function" phenotypes manifested by higher proliferative rate, greater invasive ability, and higher incidence of tumor formation. Intriguingly, we observed that an 18% increase in *AZIN1* editing was sufficient to promote tumorigenic potentials of HCC cells. All of these novel findings suggest that overediting contributes to cancer initiation and progression.

Editing of *AZIN1* induced cytoplasmic-to-nuclear translocation in HCC cells and clinical samples. Recent crystallographic and biochemical analysis of the murine antizyme inhibitor (mAzI) revealed significant conformational differences between mAzI and Odc structure lie in the two loops positioned at the dimer interface (Loop I: residues 355–362; and Loop II: 387–401)[32], suggesting these loop regions at the surface of the AzI protein are critical for maintaining its specific conformation. We identified two individual switching elements (Switch I: residues 362–367; and Switch II: residues 385–394) in AZIN1. Intriguingly, we found that the predicted AZIN1 Switch II maps to "Loop II", while Switch I element (362–367), mapping to β-strand 15 (β15), is located adjacent to "Loop I". These data suggest that the Ser367Gly editing within Switch I may induce a conformational change in AZIN1. Because a small percentage of wild-type AZIN1 protein localizes to the nucleus, the mechanism underlying the cytoplasmic-to-nuclear translocation likely does not depend solely on editing. This may explain why the AZIN1 cytoplasmic-to-nuclear change in tumor samples was not as frequently observed as overediting.

Antizyme is the first mammalian protein whose synthesis is characterized by ribosomal frame-shifting[33,34], and regulates cell growth by binding to and inducing degradation of growth promoting proteins such as ODC and CCND1. In addition, the antizyme/ODC interaction leads to a conformational alteration of ODC, thereby inducing a ubiquitin-independent proteasomal degradation of ODC[15,36]. The antizyme inhibitor AZIN1 is an ODC homologue which binds to antizyme with greater affinity than to ODC[14]. The ability of antizyme to degrade ODC, inhibit polyamine uptake, and consequently suppress cellular proliferation suggests it serves as a tumor suppressor gene. In contrast, AZIN1 prevents proteolytic degradation of ODC by sequestering antizyme from ODC. Therefore, AZIN1 acts as an oncogene by inhibiting the tumor suppressor activities of antizyme. Consistent with this model, accumulating evidence suggest that an elevated ratio of AZIN1 relative to antizyme favors growth activation. Moreover, AZIN1 levels were found to be substantially elevated in cancers of the prostate, brain, breast, and liver, and gene expression data implied alterations in the AZIN1/antizyme ratio in many human cancers[35]. In this study, we describe a third unusual mechanism of regulation of the antizyme/AZIN1 axis, that of *AZIN1* RNA editing. RNA editing of *AZIN1* confers greater antizyme binding, leading to inhibition of

degradation of target oncoproteins ODC and CCND1 and facilitating entry into the cell cycle[20,21].

Collectively, the A-to-I (G) RNA editing that occurs at codon 367 (Ser Gly) of the *AZIN1* gene, which is specifically catalyzed by *ADAR1*, is more abundant in tumor specimens. This recoding editing event is predicted to affect protein conformation, leading to changes in subcellular localization and function. Edited AZIN1, having a stronger affinity toward antizyme and a resultant higher protein stability than wild-type AZIN1, promotes cell proliferation and tumor progression by neutralizing the antizyme-mediated degradation of the ODC and CCND1 oncoproteins. Thus, HCC tumors demonstrate the increased A-to-I (G) *AZIN1* editing, leading to inhibition of antizyme tumor suppressor function providing a novel gain-of-function event driving HCC pathogenesis.

ONLINE METHODS

RNA extraction and Illumina mRNA library preparation

We selected tumor and adjacent non-tumor (NT) tissues of three HCC patients (Case No. 448, 473 and 510) in GZ cohort for RNA-Seq. Among the three individuals, two of them (448 and 473) were positive for liver cirrhosis. All three patients are HBV-positive and HCV-negative. We isolated total RNA using the mirVana™ miRNA isolation kit (Ambion, Austin, TX, USA), and treated them with the DNA-free kit (Ambion) for the removal of contaminating genomic DNA. We purified polyA$^+$ RNA using a Dynabeads mRNA purification kit (Invitrogen, Carlsbad, CA) following the manufacturer's instructions. Approximately 100 ng of mRNA was fragmented by incubation for 5 min at 94 °C in 5 × Array Fragmentation Buffer (Ambion). We synthesized double stranded cDNA using the SuperScript Double-Stranded cDNA Synthesis kit (Invitrogen) using random hexamers. The reaction was purified using a QiaQuick PCR column (Qiagen, Valencia, CA). We repaired double-stranded cDNA fragments using the DNA Terminator End Repair Kit (Lucigen, Middleton, WI) and purified them using a QiaQuick PCR column. The Klenow 3 to 5 exo- polymerase (NEB, Ipswich, MA) was used to add a single 'A' base to the 3 end of blunt phosphorylated DNA fragments. Following purification, Illumina PE Adapters (Illumina,San Diego, CA) were ligated to the ends of the DNA fragments using the Quick Ligation™ Kit (NEB, Ipswich, MA). We excised DNA fragments ranging from approximately 280 to 300 bp from a 2% low-melting agarose gel. We enriched the fragments by ten thermocycles using AccuPrime™ Pfx DNA Polymerase (Invitrogen). The PCR product was run on a Novex 8% TBE polyacrylamide gel (Invitrogen) and stained with SYBR Gold (Invitrogen). Gel slices containing the 340- to 360-bp fragments were excised and purified using the QiaQuick Gel Extraction Kit (Qiagen). We measured the concentrations of the gel-purified DNA fragments using a ND-1000 UV/Vis spectrophotometer (NanoDrop Technologies, Wilmington, DE).

RNA extraction, cDNA synthesis and quantitative real-time PCR (QPCR)

We isolated total RNA using TRIZOL Reagent (Invitrogen). To quantify gene expression levels in cells or clinical samples, equal amounts of cDNA were synthesized using the Advantage RT-for-PCR kit (Clontech, Mountain View, CA) and used for QPCR analysis. We performed QPCR using the SYBR Green PCR master mix (Applied Biosystems) and the following primers: *ADAR1*: forward, 5 CCCTTCAGCCACATCCTTC-3 ;reverse, 5 GCCATCTGCTTTGCCACTT-3 ;*ADAR2*: forward, 5 CTGACACGCTCTTCAATGGTT-3 ;reverse, 5 GGCGCAGTTCGTTCAAGAT-3 ; *AZIN1*: forward, 5 ATTGATGATGCAAACTACTCCGT-3 ;reverse, 5 GCCACTACATTCTGCCATTGA-3 ;and 18S: forward, 5 CTCTTAGCTGAGTGTCCCGC-3 ;reverse, 5 CTGATCGTCTTCGAACCTCC-3 ;For

QPCR analysis of *ADAR1* and *ADAR2* in clinical HCC samples, in addition to 18S ribosomal RNA, we used *HRPT1* (hypoxanthine phosphoribosyl-transferase I) as the other internal control with the following primers: *HRPT1*: forward, 5′-CCTGCTGGATTACATTAAAGCACTG-3′; reverse, 5′-GTCAAGGGCATATCCAACAACAAAC-3′. We performed PCR using an ABI Prism 7900 System (Applied Biosystems), and conducted data processing using the ABI SDS v2.3 software (Applied Biosystems). For cell lines, the relative *AZIN1* expression level (defined as "Relative expression") is given as $2^{-\Delta CT}$ ($\Delta C_T = C_T^{AZIN1} - C_T^{18S}$) and normalized to the relative expression level that was detected in the corresponding control cells, which was defined as 1.0. We calculated the relative expression levels of *ADAR1* and *ADAR2* in clinical HCCs and their matched NT specimens by the formula $2^{-\Delta CT}$ ($\Delta C_T = C_T^{ADAR1/ADAR2} - \text{average}[C_T^{18S} + C_T^{HPRT1}]$) and normalized to the average relative expression level in all of the NT tissues, which was defined as 1.0. When compared the ΔC_T value of *ADAR1* gene among clinical HCC, ESCC and NPC samples, we calculated the ΔC_T value by the formula $2^{-\Delta CT}$ ($\Delta C_T = C_T^{ADAR1} - C_T^{18S}$).

Solexa sequencing and read mapping

We conducted cluster generation and sequencing using the Standard Cluster Generation kit v4, and 36-Cycle Sequencing kit v3 on the Illumina Cluster Station and GAIIx following the manufacturer's instructions. We sequenced cDNA libraries from three paired HCC tumors and the corresponding NT counterparts (HCC448N/T, HCC473N/T, and HCC510N/T) with 58-base single-reads. Raw data from the GAIIx were analyzed using the Illumina Real Time Analysis (RTA) v1.6 software. A phi-X 174 control lane was included in each Solexa run for matrix, phasing, and error rate estimations as recommended by the manufacturer. The error rate of the Phi-X control error rate was < 0.28% for all of the sequencing runs.

We first removed ribosomal RNA sequences from GA reads by aligning them to 28S (NCBI RefSeq accession NR_003287.2), 18S (NCBI RefSeq accession NR_003286.2), human ribosomal DNA complete repeating unit (HSU13369) and mitochondrial ribosomal RNA (Ensembl transcript ID ENST00000387347 and ENST00000389680) using Bowtie[37] with default parameters. We then aligned the high-quality reads against the human genome assembly (NCBI Build 37.1/hg19) using TopHat v1.0.14[38] with the RefSeq refGene annotation, which was downloaded from the UCSC Genome Browser[39]. Additionally, alignment was also performed using Burrows-Wheeler Aligner v0.5.8c (BWA)[40] and CLC Genomics Workbench v4.6 (CLC bio, Denmark) to detect SNVs. Finally, we processed mapping results with custom scripts and visualized on the UCSC Genome Browser as a custom track.

Transcript assembly and abundance estimation using cufflinks

We conducted expression estimation and tests for differential expression using the Cufflinks program v0.8.3[41]. Cufflinks uses the normalized RNA-Seq fragment counts to measure relative transcript abundance. The unit of measurement is fragments per kilobase of exon per million fragments mapped (FPKM).

Variant Discovery

Briefly, we processed the aligned files from the three different software systems (see above) with SAMtools and, subsequently, with VarScan (v2.2)[42] for SNV detection. Variance calling was constrained to locations within gene regions with at least 10 × coverage, a variation frequency of greater than 30% and a base quality of more than 15. By subtracting the variation between the tumor and matched NT samples, somatic single nucleotide variations were obtained and compared with NCBI dbSNP Build 131. Finally, we

intersected the somatic SNVs detected from the three software systems to derive a set of high-confidence SNVs.

Pyrosequencing analyses of editing levels of *AZIN1*

First, we performed semi-quantitative RT-PCR using the following primers: *AZIN1*: forward, 5′-TCGCAGTTAATATCATAGC-3′; reverse, 5′-AAGGCACAAAGAAGAAGT-3′. The reverse primer was biotin labeled. Second, single-stranded biotinylated PCR products were processed for pyrosequencing analysis according to the manufacturer's standard protocol (Biotage, Qiagen Ltd, Uppsala, Sweden). Briefly, 4 μl of streptavidin-sepharose beads (Amersham Biosciences) and 29 μl of binding buffer (10 mM Tris-HCl, 1 mM EDTA, 2 M NaCl, 0.1% Tween 20, pH 7.6) were mixed with 25 μl of RT-PCR product for 10 min at room temperature. We placed the reaction mixture in a MultiScreen-HV Clear Plate (Millipore). After applying the vacuum, the beads were treated with a denaturation solution (0.2 M NaOH) for 1 min and washed twice in washing buffer (10 mM Tris-Acetate at pH 7.6). We then suspended the beads in 50 μl of annealing buffer (20 mM Tris-acetate, 2 mM Mg-acetate, pH7.6) containing 10 pmol of the sequencing primer (5′-TCCTGTGATGAGCTTGATCAA-3′). The template-sequencing primer mixture was transferred to a PSQ 96 plate (Biotage), heated to 90 °C for 2 min, and cooled to room temperature. Sequencing reactions were performed using a PSQ 96 SNP Reagent kit (Biotage), with a PSQ96MA system (Biotage) according to the manufacturer's instructions. Experiments were performed in triplicate. The sample genotype and percent heteroplasmy were determined using the allele frequency quantification (AQ) function in the SNP software (Biotage).

ADAR1 or ADAR2 overexpression assay

We amplified the full-length cDNA encoding the ADAR1 p110 isoform by PCR with primers (forward, 5′-CACCGAAAGAGGCAGGAACACCC-3′; reverse, 5′-CTATACTGGGCAGAGATAAAAGTTC-3′). The full-length cDNA encoding ADAR2 was amplified by PCR and primers (forward, 5′-CACCATGGATATAGAAGATGAAGAAAAC-3′; reverse, 5′-TCAGGGCGTGAGTGAGAACTGG-3′). The purified PCR products were ligated to the pLenti6/V5-TOPO®vector (Invitrogen) according to the manufacturer's instructions. Either the ADAR1 p110 isoform or the ADAR2 expression construct was transfected into PLC8024 cells using Lipofectamine 2000 (Invitrogen). For all transfections, empty pLenti6/V5 was used as the control vector. Thirty-six hours after transfection, the transfected cells were collected for RNA and protein extraction.

ADAR1 knockdown/rescue experiments

The *ADAR1*-specific shRNA expression vectors and the scrambled non-effective shRNA cassette in the pGFP-V-RS plasmid were purchased from OriGene Technologies, Inc (Rockville, MD). The sequences of the two shRNAs directed against *ADAR1* are as follows: sh1:CCTGTGGAATCCAGTGACATTGTGCCTAC and, sh2: AGACTCCGTACCATGTCCTGTAGTGACAA. A mixture of two pRS-shADAR1 constructs or the scrambled shRNA construct was transfected into H2M cells using Lipofectamine 2000 (Invitrogen). To generate the *ADAR1* p110 mutant construct preserving the native amino acid sequence, we introduced six mutations into the sh1 targeting sequence (29 nt). PCR-directed mutagenesis was performed using an inner forward or reverse primer containing six nucleotide alterations (forward, 5′-GAGAACGGAGAAGGCACAATCCCAGTAGAGTCAAGCGATATT-3′; reverse, 5′-AATATCGCTTGAGTCTACTGGGATTGTGCCTTCTCCGTTCTC-3′) with the corresponding external primer.

Twenty-four hours after transfection, the transfected cells were cultured for 3 days with 1 μg ml^{-1} puromycin (OriGene). Pooled populations of knockdown/rescue cells were subjected to *in vitro* experiments.

Prediction of conformational switching elements

We analyzed the conformational switching elements using the predictProtein Server (CUBIC, Biochemistry, Columbia University, New York) and the Ambivalent Structure Predictor (ASP)[13]. ASP was designed to identify the location of conformational switches in amino acid sequences and analyzed results from a secondary structure prediction algorithm to identify regions of conformational ambivalence. To better interpret our output, please see Young et al., Protein Science 8(9):1852–64. 1999[13] for details. The full length crystal structure of human AZIN1 (PDB id: 3BTN) was used as template for visualizing 3D protein structure generated by PyMOL program (Delano Scientific).

Lentiviral expression system

We generated stably expressed wild-type or edited *AZIN1*, which was fused in frame with a V5 epitope tag, using the pLenti6/V5-TOPO®vector (Invitrogen) according to the manufacturer's instructions. Either the *AZIN1* expression construct or the *LacZ* control plasmid was transfected into the 293FT cell line. Virus-containing supernatants were collected for subsequent transduction into QGY7703 and PLC8024 cells. Blasticidin (20 μg ml^{-1}; Sigma-Aldrich) was used to select for stably transduced cells.

Western blot analysis and antibodies

Protein lysates were quantified and resolved on a SDS-PAGE gel, transferred onto a polyvinylidene difluoride (PVDF) membrane (Millipore, Billerica, MA, USA), and immunoblotted with a primary antibody, followed by incubation with a secondary antibody. The blots were visualized by enhanced chemiluminescence (GE Healthcare, Buckinghamshire, UK). The following antibodies were used: antibodies to ODC (1:2,000, Abcam, ab66067), AZIN1 (1:2,000, Abcam, ab57169), β-actin (1:5,000, Abcam, ab6276), GAPDH (1:3,000, Thermo, MA5-15738), AZIN1 (1:1,000, Abcam, ab57169), ADAR1 (1:2,000, Abcam, ab88574), ADAR2 (1:1,000, Sigma-Aldrich, SAB1405426), β-tubulin (1:1000, Santa Cruz Biotechnology, sc-5286), Lamin A/C (1:2,000, Santa Cruz Biotechnology, sc-6215), cyclin A2 (1:1,000, Cell Signaling Technology, 4656), cyclin D1 (1:1,000, Cell Signaling Technology, 2926), total Rb (1:1,000, Cell Signaling Technology, 9313), and phosphor/Rb (ser807/811) (1:1,000, Cell Signaling Technology, 9308), GFP (1:2,000, Santa Cruz Biotechnology, sc-9996), antizyme-1 (1:10,000, Sigma-Aldrich, SAB4502039) and V5 (1:1,000, Serotec, MCA1360GA). The ImageJ program (available at http://rsb.info.nih.gov/ij) was used for densitometric analyses of western blots, and the quantification results were normalized to the loading control.

Immunohistochemical staining (IHC)

We sectioned the paraffin-embedded tissue blocks for IHC staining. Briefly, sections were deparaffinized and rehydrated. The endogenous peroxidase activity was blocked with 3% hydrogen peroxide (H_2O_2) for 10 min. For antigen retrieval, the slides were immersed in 10 mM citrate buffer (pH 6.0) and boiled for 15 min in a microwave oven. Non-specific binding was blocked with 5% normal goat serum for 10 min. The slides were incubated in a 1:200 dilution of AZIN1-specific antibody (Abcam, ab57169) at 4 °C overnight in a humidified chamber. The slides were then sequentially incubated with biotinylated goat anti-mouse IgG (1:100, Santa Cruz, sc-2039) for 30 min at room temperature, followed by streptavidin-peroxidase conjugate for 30 min at room temperature. Finally, the 3, 5-

diaminobenzidine (DAB) Substrate Kit (Dako) was used for color development followed by Mayer's hematoxylin counterstaining.

Foci formation and colony formation in soft agar assays

For the foci formation assay, 1×10^3 cells were seeded in a 6-well plate. After culture for 7 days, surviving colonies (> 50 cells per colony) were counted and stained using crystal violet (Sigma-Aldrich). Triplicate independent experiments were performed. For colony formation in soft agar, 5×10^3 cells in 0.4% bacto agar were seeded on top of a solidified layer of 0.6% bacto agar in 6-well plates. Colonies consisting of more than 50 cells were counted after 3 weeks, and the data were expressed as the mean ± s.e.m of triplicate wells within the same experiment.

Matrigel Invasion assay

We performed invasion assays using 24-well BioCoat Matrigel Invasion Chambers (BD Biosciences) according to the manufacturer's instructions. Briefly, 2×10^5 cells were added to the top chamber, and 10% FBS in DMEM was added to the bottom chamber as a chemoattractant. After 30 hours of incubation, cells that invaded the Matrigel were fixed and stained with crystal violet (Sigma-Aldrich). The number of cells was counted in 10 fields under a 20 × objective lens and imaged using SPOT imaging software (Nikon, Japan).

In vivo tumorigenicity assay

Subcutaneous injection: We subcutaneously injected approxiamtely 1×10^6 cells into the right flank of 4- to 5- week-old male severe combined immunodeficient (SCID) mice. We monitored tumor formation in the SCID mice over a 4-week period and calculated the tumor volume weekly by the formula V (volume) = 0.5 × L (length) × W (width) × W[43]. Intrahepatic injection: Under sterile conditions, a midline abdominal incision was made to expose the lateral left lobe of the liver. Approxiamtely 1×10^6 cells were delivered via a direct intrahepatic injection into the liver parenchyma. Four weeks post-injection, the number of tumor nodules greater than 1 mm in diameter was counted. All animal experiments were approved by and performed in accordance with the Institutional Animal Care and Use Committees of the University of Hong Kong and National University of Singapore.

Xenograft tumor processing

We washed xenograft tumor samples in DMEM supplemented with 100% FBS. After rinsing in the same medium twice, tumor tissues were minced into 1 mm^3 pieces and incubated with 1× Accumax (1,200–2,000 U ml^{-1} proteolytic activity containing collagenase and DNase (Innovative Cell Technologies, Inc., San Diego, CA) at 10 ml g^{-1} tissue in PBS for 20 min at 37 °C under constant rotation. A single cell suspension was obtained by filtering the supernatant through a 100 μmol l^{-1} strainer, followed by a 40 μmol l^{-1} cell strainer (BD Biosciences, San Jose, CA).

Bromodeoxyuridine (BrdU) Incorporation assay

To synchronize cells at the G0/G1 phase, we treated cells with mimosine (400 μmol l^{-1}; Sigma-Aldrich) for 24 hours (0 h) and then released into complete medium containing BrdU (1 μmol l^{-1}) for 6 (6 h) or 9 (9 h) hours. The proportion of cells entering S phase was assessed by flowcytometric analysis of BrdU incorporation using the APC BrdU Flow kit (Becton Dickinson Biosciences) following the manufacturer's instructions. The R4 region captures the S-phase populations (positive for BrdU incorporation).

Co-immuoprecipitation (Co-IP)

PLC8024 cells were transfected with 2.0 μg of the GFP-tagged wild-type or edited *AZIN1* plasmid (GFP-wt/AZI or GFP-edt/AZI). In addition, the 8024-edt/AZI or 8024-wt/AZI stable cell lines were also analyzed via Co-IP assay using a V5-specific antibody. Approximately 10 mg of total cell lysate was immunoprecipitated with 5 μg of V5-specific or GFP-specific antibodies at 4 °C for 4 hours. Immunocomplexes were then precipitated using 100 μl of protein G-agarose, which was provided in the immunoprecipitation kit (Roche Diagnostics Co., Indianapolis, IN). After an extensive washing in washing buffer, the beads were boiled in 50 μl of loading buffer and analyzed by Western blot analysis using antibodies against GFP, V5 and antizyme-1. We utilized 5% of the whole lysates (5% Input) as a positive control. Mouse immunoglobulin G (Santa Cruz Biotechnology) was used as a negative control.

In vitro binding assay

Recombinant antizyme-1 (OAZ1) was expressed as a protein fused to maltose-binding protein (MBP) (MBP-OAZ1). The expression of MBP-OAZ1 or MBP in BL21 (DE3) *E. coli* was induced by incubation with 0.1 mmol l^{-1} IPTG at 37 °C for 6 hours. Cell pellets were lysed in fresh MBP binding buffer. After centrifugation, the samples were incubated with amylose-agarose resin at 4 °C overnight. After washing with 200 volumes of MBP binding buffer, either MBP-OAZ1 or MBP resin was added to the whole HEK293T cell lysate, which was transfected with an equal amount (8.0 μg) of GFP-wt/AZI or GFP-edt/AZI expression constructs. After incubation at 4 °C overnight, the resin was washed with 200 volumes of MBP binding buffer, boiled in 1 volume of 2 × SDS loading buffer and analyzed by Western blot analysis using a GFP-specific antibody.

Supplementary Material

Refer to Web version on PubMed Central for supplementary material.

Acknowledgments

We thank and acknowledge the patients for tumor tissue donation to our tissue bank and M. Fullwood for providing cDNA samples of normal individual tissues. This work was supported by the Hong Kong Research Grant Council grants including Theme-based Research Scheme Fund (T12-403/11), Collaborative Research Funds (HKBU5/CRF/10, HKU7/CRG/09, and HKU3/CRF/11R), and General Research Fund (HKU/766811M), China National Basic Research Program (2012CB967001), “Hundred Talents Program” at Sun Yat-Sen University (85000-3171311), and the China National Key Science-Technology Special Project of Infectious Diseases (2008ZX10002-022), and the Singapore Ministry of Health’s National Medical Research Council under its Singapore Translational Research (STaR) Investigator Award.

References

1. Parkin DM, Bray F, Ferlay J, Pisani P. Global cancer statistics, 2002. CA Cancer J Clin. 2005; 55:74–108. [PubMed: 15761078]
2. Farazi PA, DePinho RA. Hepatocellular carcinoma pathogenesis: from genes to environment. Nat Rev Cancer. 2006; 6:674–687. [PubMed: 16929323]
3. Thorgeirsson SS, Grisham JW. Molecular pathogenesis of human hepatocellular carcinoma. Nat Genet. 2002; 31:339–346. [PubMed: 12149612]
4. Meyerson M, Gabriel S, Getz G. Advances in understanding cancer genomes through second-generation sequencing. Nat Rev Genet. 11:685–696. [PubMed: 20847746]
5. Morozova O, Marra MA. Applications of next-generation sequencing technologies in functional genomics. Genomics. 2008; 92:255–264. [PubMed: 18703132]
6. Wang Z, Gerstein M, Snyder M. RNA-Seq: a revolutionary tool for transcriptomics. Nat Rev Genet. 2009; 10:57–63. [PubMed: 19015660]

7. Bass BL. RNA editing by adenosine deaminases that act on RNA. Annu Rev Biochem. 2002; 71:817–846. [PubMed: 12045112]
8. Herb A, Higuchi M, Sprengel R, Seeburg PH. Q/R site editing in kainate receptor GluR5 and GluR6 pre-mRNAs requires distant intronic sequences. Proc Natl Acad Sci U S A. 1996; 93:1875–1880. [PubMed: 8700852]
9. Higuchi M, et al. RNA editing of AMPA receptor subunit GluR-B: a base-paired intron-exon structure determines position and efficiency. Cell. 1993; 75:1361–1370. [PubMed: 8269514]
10. Samuel CE. Antiviral actions of interferons. Clinical microbiology reviews. 2001; 14:778–809. table of contents. [PubMed: 11585785]
11. Farajollahi S, Maas S. Molecular diversity through RNA editing: a balancing act. Trends Genet. 2010; 26:221–230. [PubMed: 20395010]
12. Mangold U, Hayakawa H, Coughlin M, Munger K, Zetter BR. Antizyme, a mediator of ubiquitin-independent proteasomal degradation and its inhibitor localize to centrosomes and modulate centriole amplification. Oncogene. 2008; 27:604–613. [PubMed: 17667942]
13. Young M, Kirshenbaum K, Dill KA, Highsmith S. Predicting conformational switches in proteins. Protein science: a publication of the Protein Society. 1999; 8:1752–1764. [PubMed: 10493576]
14. Fujita K, Murakami Y, Hayashi S. A macromolecular inhibitor of the antizyme to ornithine decarboxylase. Biochem J. 1982; 204:647–652. [PubMed: 7126159]
15. Mangold U. Antizyme inhibitor: mysterious modulator of cell proliferation. Cell Mol Life Sci. 2006; 63:2095–2101. [PubMed: 16847581]
16. Bercovich Z, Kahana C. Degradation of antizyme inhibitor, an ornithine decarboxylase homologous protein, is ubiquitin-dependent and is inhibited by antizyme. J Biol Chem. 2004; 279:54097–54102. [PubMed: 15491992]
17. Kahana C. Antizyme and antizyme inhibitor, a regulatory tango. Cell Mol Life Sci. 2009; 66:2479–2488. [PubMed: 19399584]
18. Newman RM, et al. Antizyme targets cyclin D1 for degradation. A novel mechanism for cell growth repression. J Biol Chem. 2004; 279:41504–41511. [PubMed: 15277517]
19. Vivanco I, Sawyers CL. The phosphatidylinositol 3-Kinase AKT pathway in human cancer. Nat Rev Cancer. 2002; 2:489–501. [PubMed: 12094235]
20. Morgan DO. Principles of CDK regulation. Nature. 1995; 374:131–134. [PubMed: 7877684]
21. Pyronnet S, Pradayrol L, Sonenberg N. A cell cycle-dependent internal ribosome entry site. Mol Cell. 2000; 5:607–616. [PubMed: 10882097]
22. Lukas J, Petersen BO, Holm K, Bartek J, Helin K. Deregulated expression of E2F family members induces S-phase entry and overcomes p16INK4A-mediated growth suppression. Mol Cell Biol. 1996; 16:1047–1057. [PubMed: 8622649]
23. Gommans WM, Mullen SP, Maas S. RNA editing: a driving force for adaptive evolution? Bioessays. 2009; 31:1137–1145. [PubMed: 19708020]
24. Mattick JS, Mehler MF. RNA editing, DNA recoding and the evolution of human cognition. Trends in neurosciences. 2008; 31:227–233. [PubMed: 18395806]
25. Reenan RA. Molecular determinants and guided evolution of species-specific RNA editing. Nature. 2005; 434:409–413. [PubMed: 15772668]
26. Li JB, et al. Genome-wide identification of human RNA editing sites by parallel DNA capturing and sequencing. Science. 2009; 324:1210–1213. [PubMed: 19478186]
27. Shah SP, et al. Mutational evolution in a lobular breast tumour profiled at single nucleotide resolution. Nature. 2009; 461:809–813. [PubMed: 19812674]
28. Cenci C, et al. Down-regulation of RNA editing in pediatric astrocytomas: ADAR2 editing activity inhibits cell migration and proliferation. J Biol Chem. 2008; 283:7251–7260. [PubMed: 18178553]
29. Maas S, Patt S, Schrey M, Rich A. Underediting of glutamate receptor GluR-B mRNA in malignant gliomas. Proc Natl Acad Sci U S A. 2001; 98:14687–14692. [PubMed: 11717408]
30. Paz N, et al. Altered adenosine-to-inosine RNA editing in human cancer. Genome Res. 2007; 17:1586–1595. [PubMed: 17908822]

31. Gallo A, Galardi S. A-to-I RNA editing and cancer: from pathology to basic science. RNA Biol. 2008; 5:135–139. [PubMed: 18758244]
32. Albeck S, et al. Crystallographic and biochemical studies revealing the structural basis for antizyme inhibitor function. Protein science: a publication of the Protein Society. 2008; 17:793–802. [PubMed: 18369191]
33. Matsufuji S, et al. Autoregulatory frameshifting in decoding mammalian ornithine decarboxylase antizyme. Cell. 1995; 80:51–60. [PubMed: 7813017]
34. Rom E, Kahana C. Polyamines regulate the expression of ornithine decarboxylase antizyme in vitro by inducing ribosomal frame-shifting. Proc Natl Acad Sci U S A. 1994; 91:3959–3963. [PubMed: 8171019]
35. Olsen RR, Zetter BR. Evidence of a role for antizyme and antizyme inhibitor as regulators of human cancer. Molecular cancer research: MCR. 2011; 9:1285–1293. [PubMed: 21849468]
36. Hu L, et al. Association of Vimentin overexpression and hepatocellular carcinoma metastasis. Oncogene. 2004; 23:298–302. [PubMed: 14647434]
37. Langmead B, Trapnell C, Pop M, Salzberg SL. Ultrafast and memory-efficient alignment of short DNA sequences to the human genome. Genome Biol. 2009; 10:R25. [PubMed: 19261174]
38. Trapnell C, Pachter L, Salzberg SL. TopHat: discovering splice junctions with RNA-Seq. Bioinformatics. 2009; 25:1105–1111. [PubMed: 19289445]
39. Zweig AS, Karolchik D, Kuhn RM, Haussler D, Kent WJ. UCSC genome browser tutorial. Genomics. 2008; 92:75–84. [PubMed: 18514479]
40. Li H, Durbin R. Fast and accurate short read alignment with Burrows-Wheeler transform. Bioinformatics. 2009; 25:1754–1760. [PubMed: 19451168]
41. Trapnell C, et al. Transcript assembly and quantification by RNA-Seq reveals unannotated transcripts and isoform switching during cell differentiation. Nat Biotechnol. 2010; 28:511–515. [PubMed: 20436464]
42. Koboldt DC, et al. VarScan: variant detection in massively parallel sequencing of individual and pooled samples. Bioinformatics. 2009; 25:2283–2285. [PubMed: 19542151]
43. Cao ZA, Daniel D, Hanahan D. Sub-lethal radiation enhances anti-tumor immunotherapy in a transgenic mouse model of pancreatic cancer. BMC cancer. 2002; 2:11. [PubMed: 12019035]

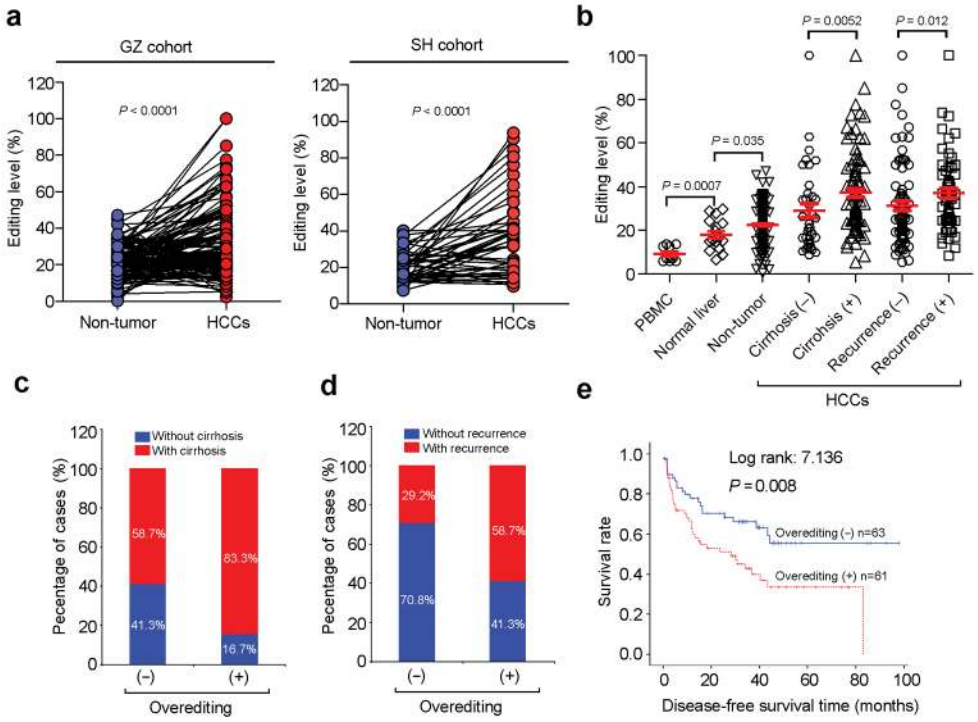

Figure 1.

AZIN1 overediting is strongly associated with HCC pathogenesis. (**a**) *AZIN1* editing levels in HCC and matched non-tumor (NT) liver specimens from 135 and 46 patients in the Guangzhou (GZ) (left panel) and Shanghai (SH) cohorts (right panel), respectively (paired Student's *t*-test). (**b**) Dot plots represent *AZIN1* editing levels in healthy human peripheral blood mononuclear cells (PBMCs) (n = 10), healthy human liver tissues (n = 20), and adjacent NT liver specimens of 135 patients with HCC from the GZ cohort (Mann-Whitney U test). Matched HCC specimens were subdivided into four categories according to the presence of cirrhosis or tumor recurrence. (**c**) Association between presence of liver cirrhosis and *AZIN1*overediting (*chi*-square test). (**d**) Association between recurrence incidence and *AZIN1* overediting (*chi*-square test). (**e**) Kaplan-Meier plots for the disease-free survival rate of patients with HCC in "overediting (+)" and "overediting (−)" groups (Log rank test).

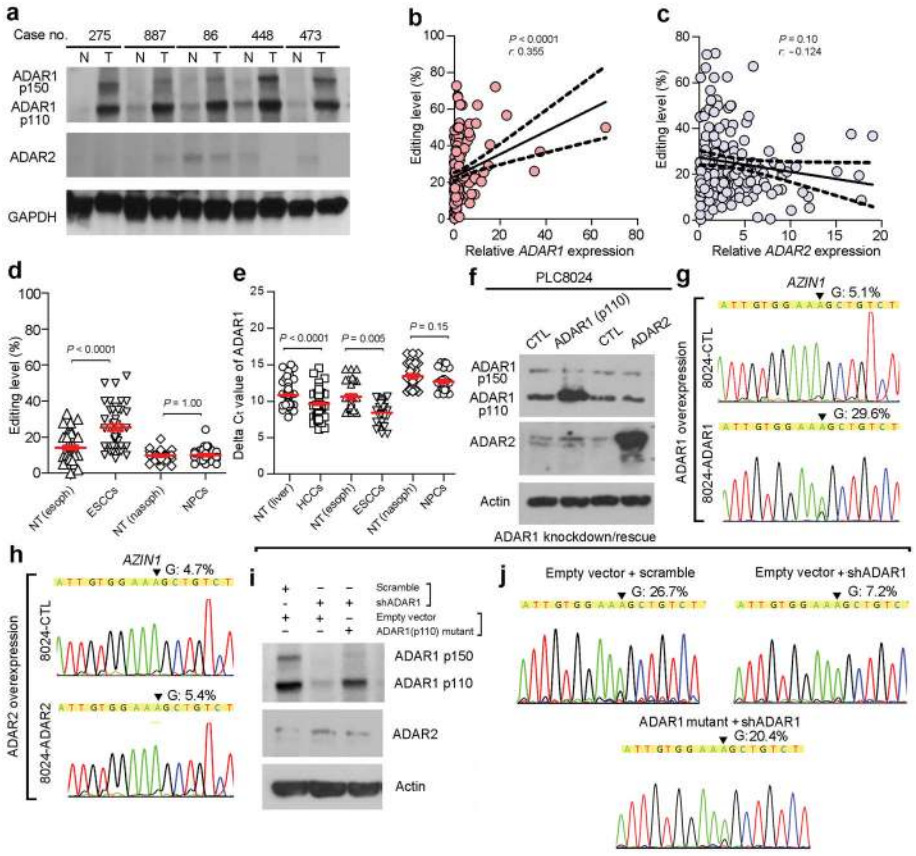

Figure 2.

ADAR1 directs A-to-I *AZIN1* RNA Editing. (**a**) Western blot showing expression of ADAR1 and ADAR2 proteins in HCC (T) and matched non-tumor liver (N) (Case No. 275, 887, 86, 448, and 473) specimens. GAPDH is the loading control. (**b, c**) Correlation between relative RNA levels of *ADAR1* (**b**) and *ADAR2* (**c**) and *AZIN1* editing in tumor and NT specimens from 94 patients with HCC in the GZ cohort, expressed using Spearman correlation coefficients, linear regression (solid lines), and the 95% confidence interval (dotted lines). (**d**) Dot plots representing the *AZIN1* editing in ESCC and NPC and in paired NT samples by pyrosequencing (ESCCs: n = 43; NPCs: n = 33; Mann-Whitney U test). (**e**) Dot plots representing the delta Ct (Ct) values of *ADAR1* in the same samples described in (**b**) and (**d**) by QPCR (Mann-Whitney U test). (**f**) Western blot showing expression of ADAR1 and ADAR2 proteins in PLC8024 cells transiently transfected with the indicated expression constructs. (**g, h**) Sequence chromatograms of the *AZIN1* transcript in the indicated cell lines; the arrow indicates the edited position. (**i**) Western blot of ADAR1 and ADAR2 in H2M cells transiently transfected with expression plasmids as indicated. (**j**) Sequence chromatograms of the *AZIN1* transcript in the indicated cell lines. The percentage of edited *AZIN1* transcripts was detected by pyrosequencing. An arrow indicates the editing position.

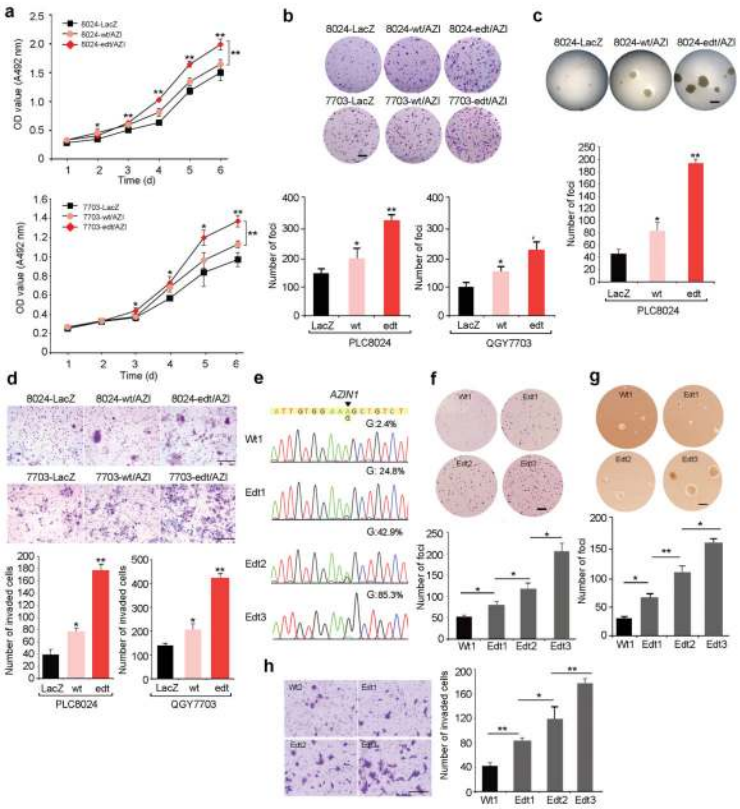

Figure 3.

AZIN1 RNA editing confers enhanced tumorigenicity. (**a**) XTT assays showing growth rates of the indicated stable cell lines. (*, $P < 0.05$; **, $P < 0.01$). (**b**) Quantification of foci formation induced by the indicated stable cell lines (*, $P < 0.05$; **, $P < 0.001$). Scale bar: 0.5 cm. (**c**) Quantification of soft agar colonies induced by the indicated stable cell lines (*, $P < 0.05$; **, $P < 0.001$). Scale bar: 100 □m. (**d**) Quantification of cells from the indicated stable cells that invaded through Matrigel-coated membrane (*, $P < 0.05$; **, $P < 0.001$). (**e**) Direct sequencing of the *AZIN1* transcripts from the indicated cell lines. The percentage of edited *AZIN1* transcripts was determined by pyrosequencing. An arrow indicates the editing position. (**f, g**) Quantification of foci formation (**f**) and colony formation in soft agar (**g**) induced by 8024-Wt1, Edt1, Edt2 and Edt3 cells (*, $P < 0.05$; **, $P < 0.001$). Scale bar: **f**, 1 cm; **g**, 100 □m. (**h**) Quantification of cells from the indicated stable cells that invaded through Matrigel-coated membrane (*, $P < 0.05$; **, $P < 0.001$). Scale bar: 200 □m. For all panels, data are presented as mean ± s.e.m of three independent experiments and statistical significance determined by unpaired, two-tailed Student's *t* test.

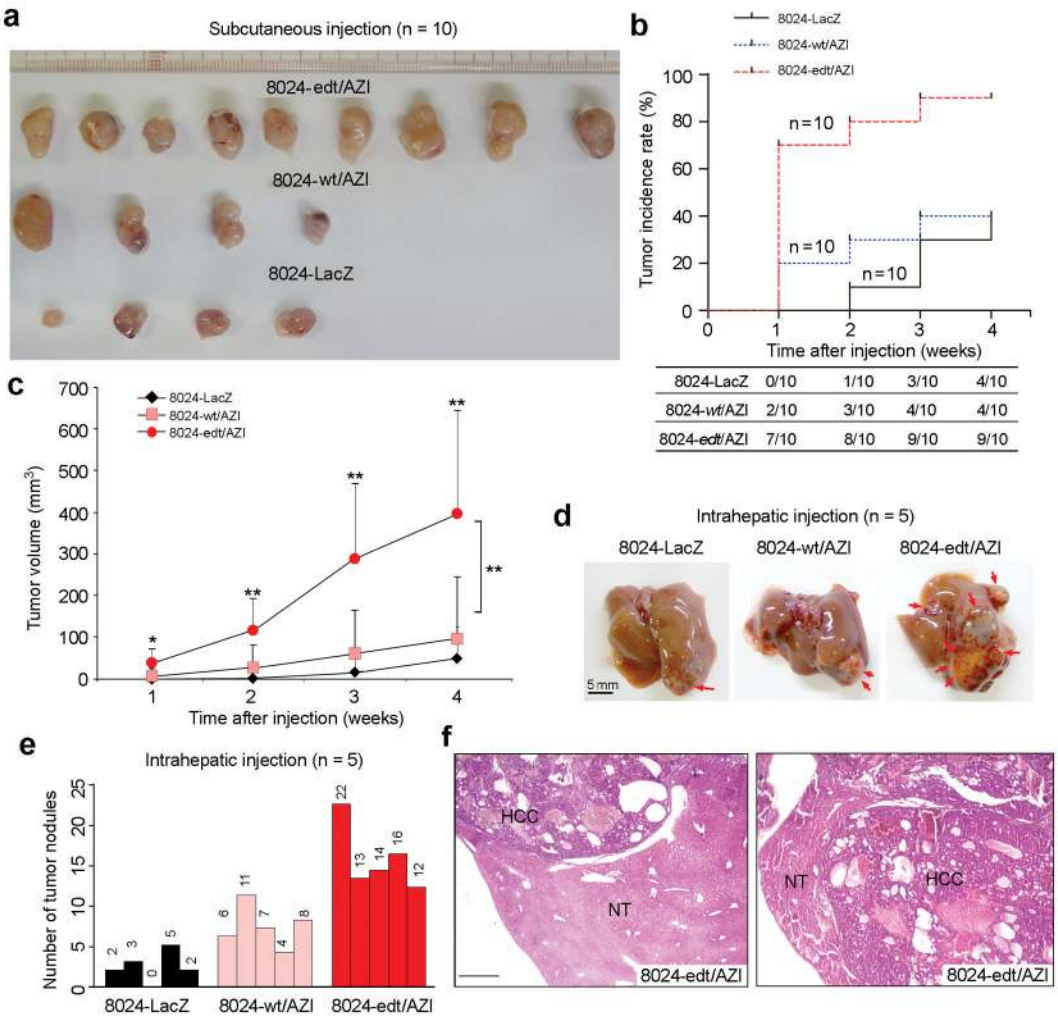

Figure 4.

AZIN1 editing contributes to augmented tumor initiating potential and enhanced *in vivo* tumorigenic ability. (**a**) Tumors derived from 8024-LacZ, 8024-wt/AZI and 8024-edt/AZI cells 4 weeks post subcutaneous injection (n = 10 per group). (**b**) Cumulative tumor incidence curves of severe combined immunodeficient (SCID) mice from the indicated cell lines estimated by the Kaplan-Meier method. (**c**) Growth curves of tumors derived from the indicated cell lines over a period of 4 weeks (*, $P<0.05$; **, $P<0.01$). Statistical significance was determined by unpaired, two-tailed Student's *t* test. (**d**) Representative images of mouse livers that underwent intrahepatic inoculation with 8024-wt/AZI, 8024-edt/AZI and 8024-LacZ cells 4 weeks post-injection (n = 5). Arrows indicate focal tumor nodules on liver surfaces. Scale bar: 5 mm. (**e**) The numbers of tumor nodules (larger than 1 mm in diameter). (**f**) H&E staining showing severe HCC lesions in 8024-edt/AZI-injected livers. NT, adjacent non-tumor. Scale bar: 200 μm.

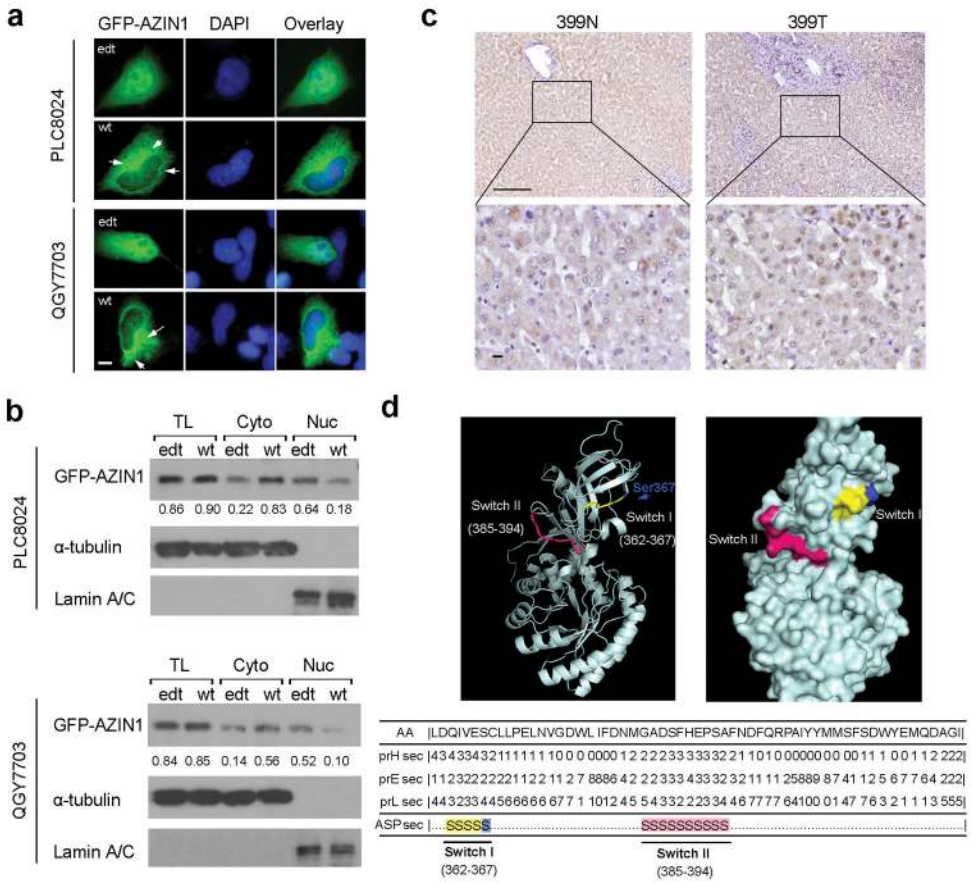

Figure 5.

RNA editing of *AZIN1* changes subcellular localization. (**a**) GFP-tagged wild-type or edited AZIN1 protein expressed in QGY7703 and PLC8024 cells. Images on the right are the overlay of GFP-tagged AZIN1 and nuclear DAPI (blue) staining of the same field. Arrows indicate centrosomal localization of wild-type AZIN1 protein. Scale bar, 10 □n. (**b**) Western blot of GFP-tagged wild-type and edited AZIN1 protein in the total lysate (TL), cytoplasmic (Cyto), and nuclear (Nuc) fractions of PLC8024 and QGY7703 cells transfected with GFP-wt/AZI or GFP-edt/AZI constructs. Lamin A/C and □-tubulin are loading controls for nuclear and cytoplasmic fractions, respectively. (**c**) Immunohistochemical (IHC) staining of AZIN1 for a pair of tumor (399T) and matched NT (399N) tissues from HCC patient (Case No. 399) with *AZIN1* overediting in the tumor. The boxed regions are magnified and shown in the lower panels. Scale bar, 200 □n. (**d**) Predicted conformational switch regions of AZIN1 protein. Lower panel: Two predicted individual switching elements (Switch I and Switch II)[13]. Switch I comprises residues 362–367 (yellow); residue Ser367 corresponding to the edited codon is highlighted in blue; Switch II comprises residues 385–394 (pink). Upper-left panel: Ribbon drawing; Upper-right panel: Surface diagram.

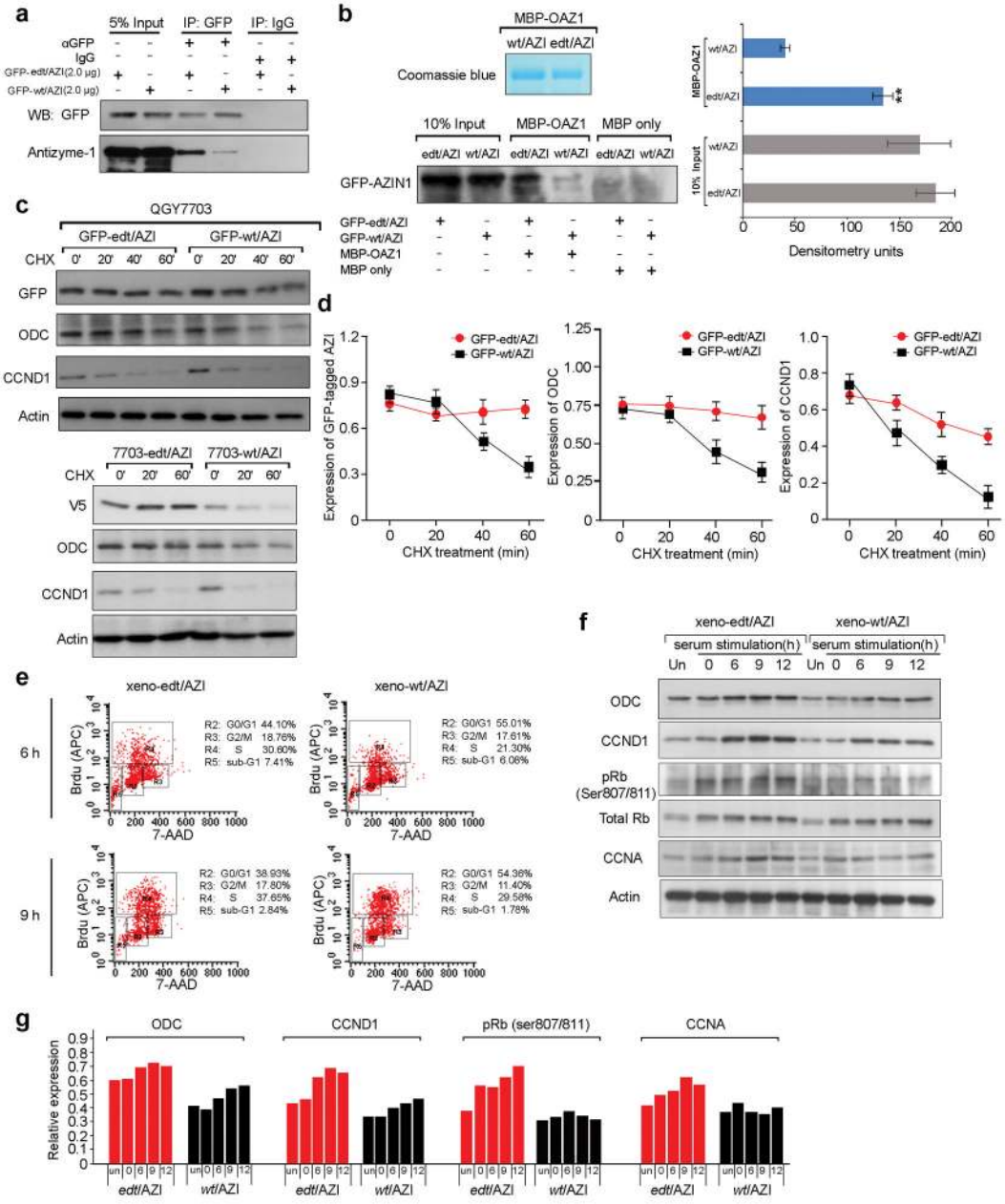

Figure 6.

Edited AZIN1 neutralizes antizyme-mediated degradation of target oncoproteins *in vitro* and *in vivo*. (**a**) Co-immunoprecipitation of antizyme-1 in PLC8024 cells transfected with the indicated constructs using a GFP-specific antibody (IP: GFP) or mouse IgG (IP: IgG). (**b**) Western blot of GFP-tagged AZIN1 showing the binding affinities of wild-type and edited AZIN1 protein to maltose-binding protein (MBP)-fused antizyme-1 (MBP-OAZ1) or MBP resin beads (MBP only). "10% Input" indicates 10% of whole cell lysates from HEK293T cells transfected with the indicated constructs. Data are presented as mean ± s.e.m of three independent experiments and statistical significance determined by unpaired, two-tailed Student's *t* test (**, $P < 0.00001$). (**c, d**) Western blot demonstrating expression of tagged AZIN1, ODC, and CCND1 in QGY7703 cells transfected with GFP-edt/AZI or GFP-wt/AZI or in stable cell lines (7703-edt/AZI and 7703-wt/AZI) after cycloheximide (CHX) treatment

(50 μg ml^{-1}) for the indicated times in minutes. Data are presented as mean ± s.e.m of three independent experiments (**d**). (**e**) Scatter plots of fluorescence intensities of BrdU incorporation (APC anti-BrdU, Y axis) against DNA content (7-AAD, X-axis) for each cell line at 6 and 9 hours after release. (**f, g**) Western blot of ODC, CCND1, pRb, total Rb, and CCNA in xeno-wt/AZI and xeno-edt/AZI cells at each time point. Protein levels were quantified and expressed as the average of two independent experiments (**g**).